Electronic properties of GaAsBi(001) alloys at low Bi content

J. Honolka,[1] C. Hogan,[2,3] M. Vondráček,[1] Y. Polyak,[1] F. Arciprete,[3,2] and E. Placidi[2,3]
[1]*Institute of Physics, Academy of Sciences of the Czech Republic, Na Slovance 2, CZ-182 21 Praha 8, Czech Republic*
[2]*Istituto di Struttura della Materia-CNR (ISM-CNR), Via del Fosso del Cavaliere 100, 00133 Roma, Italy*
[3]*Università di Roma "Tor Vergata", Dipartimento di Fisica, via della Ricerca Scientifica 1, 00133 Roma, Italy*

(Received 13 August 2018; published 5 April 2019; corrected 23 March 2022)

We present an in-depth investigation of structural and electronic properties of GaAsBi epilayers. High (001) crystalline order is achieved using careful molecular beam epitaxy and surface preparation procedures. High surface order allows us to use x-ray, ultraviolet, and angle-resolved photoemission spectroscopy at variable photon energies and to disentangle electronic effects of an atomically thin Bi-rich surface layer with (2×3) symmetry from those of Bi atoms incorporated in the GaAs bulk matrix. The influence of bulk-integrated Bi concentrations on the GaAs band structure becomes visible in angle-resolved photoemission after removing Bi-rich surface layers by a brief and mild ion bombardment and subsequent annealing treatment. Experimental observations are supported by density functional theory simulations of the valence band structure of bulk and surface-reconstructed GaAs with and without Bi. Bi-induced energy shifts in the dispersion of GaAs heavy and light hole bulk bands are evident both in experiment and theory, which are relevant for modulations in the optical band gap and thus optoelectronic applications.

DOI: 10.1103/PhysRevMaterials.3.044601

I. INTRODUCTION

$GaAs_{1-x}Bi_x$ alloys have enormous potential for advanced applications in the fields of electronics, optoelectronics, nanophotonics, thermoelectricity, and photovoltaics [1–3]. The incorporation of Bi into GaAs induces a large band-gap bowing, even at Bi concentrations less than few percent [4] due to a large upward shift of the valence band edge. This property offers a large freedom to engineer the alloy's band structure towards potential high-speed electronic and infrared optoelectronic applications: Bi alloying in $GaAs_{1-x}Bi_x$ seems to improve the hole mobility while preserving the high electron mobility of GaAs [5].

Despite the strategic interest in $GaAs_{1-x}Bi_x$, reliable growth procedures leading to high-quality material properties are missing for several reasons. The existence of a large miscibility gap requires low growth temperatures leading to the formation of defects that degrade the optical properties. Moreover, the surfactant action of Bi counteracts a homogeneous incorporation; phase-separation phenomena can occur, like the formation of Ga-Bi droplets on the surface or modulations of Bi compositions in the bulk [6], whose connection to growth conditions and to optical properties is not yet understood.

To understand the influence of Bi on optical and electronic band structure properties of $GaAs_{1-x}Bi_x$ alloys it is essential to improve their bulk and surface crystal qualities, which would eventually allow also cutting edge band structure analysis techniques like momentum-resolved photoemission spectroscopy.

In this paper we investigate the structure and electronic valence band properties of GaAsBi alloys for varying Bi concentrations. $GaAs_{1-x}Bi_x$ epilayers with high crystalline order are grown by molecular beam epitaxy (MBE) on GaAs(001) single crystal substrates. Bi inclusion in the GaAs lattice is studied by means of x-ray photoemission spectroscopy (XPS). Due to high surface crystalline order of MBE-grown films, Bi-induced effects on the electronic band structure can be studied using ultraviolet photoemission spectroscopy (UPS) and k-resolved photoemission electron microscopy (k-PEEM). Our results show Bi integration in two different states. One corresponds to a Bi-rich surface layer. The second phase corresponds to Bi atoms integrated in the bulk with concentrations up to 1.3%, which is essential for bulk-related applications, such as optoelectronics. Band structures are interpreted by means of density functional theory (DFT) calculations of the electronic properties of bulk GaAs and $\beta 2(2 \times 4)$-reconstructed slab geometries with and without subsurface incorporation of Bi. The presence of Bi induces small energetic shifts and considerable distortions on the lineshapes, in good agreement with experimental observations.

The paper is organized as follows. Section II reports the sample preparation procedure, experimental methodology, and DFT calculations. XPS studies are given in Sec. III. Section IV reports our measured k-PEEM data and theoretical analysis of the band structures for pristine and GaAsBi GaAs(001), respectively. More precise analysis of surface-related features obtained via UPS is given in Sec. V. The paper concludes with a short summary.

II. METHODOLOGY

A. Sample preparation procedure and experimental methods

Pure GaAs and GaAsBi samples were grown by MBE on n(Si)-doped (10^{18} cm^{-3}) GaAs(001) substrates with a miscut angle of about 0.01°. GaAs buffer layers of approximate 500-nm thickness were grown at 590° C. For the growth of GaAsBi layers, the substrate temperature was decreased to

 ©2019 American Physical Society

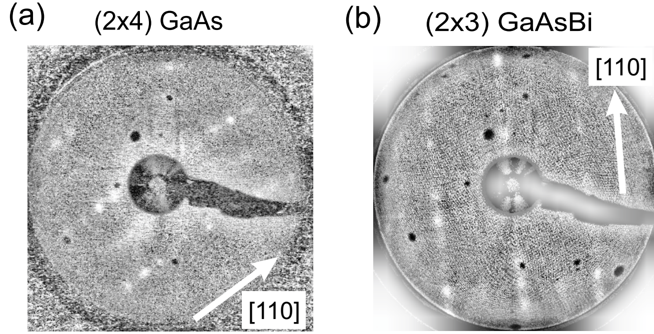

FIG. 1. LEED images for (a) as-grown (2 × 4) GaAs(001) and (b) sputter-annealed $GaAs_{1-x}Bi_x$ ($x = 2.7\%$) with a (2 × 3) surface reconstruction.

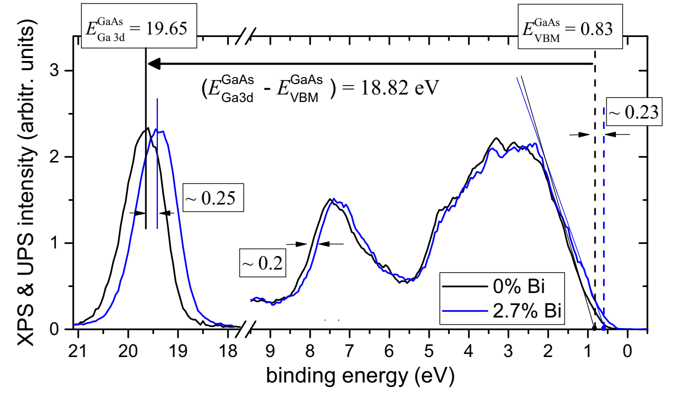

FIG. 2. Valence band spectra and shallow Ga 3*d* CLs measured at 1.5 keV. Data for GaAs (2 × 4) (black) and $GaAs_{1-x}Bi_x$ (x = 2.7%) (blue) after decapping are plotted. Values of E_{VBM}^{GaAs} and E_{VBM}^{GaAsBi} were derived using the leading edge method indicated by the tangential dashed lines.

325° C. A layer of 150 nm of $GaAs_{1-x}Bi_x$ was deposited at a flux rate of 0.5 ML/s. The Bi concentration x in units [%] was estimated by Bi flux calibration and confirmed by high-resolution x-ray diffraction. At the end of both GaAs and GaAsBi epilayer deposition, samples were cooled down to about −10° C, and an amorphous As capping layer was deposited to prevent the sample from contamination during air exposure when *ex situ* shipped to external analysis facilities.

Prior to surface sensitive LEED, XPS, and *k*-PEEM measurements, the samples were decapped *in situ* under ultrahigh vacuum (UHV) conditions at temperatures of 300° C and subsequently annealed at 400–440° C. Temperatures were monitored directly on the sample using an optical pyrometer. Resulting surface order was investigated by LEED where a (2 × 4) pattern is found for pure GaAs(001) as shown in Fig. 1(a). On the other hand, GaAsBi samples showed much weaker LEED structures according to a (2 × 3) pattern. We will refer to these samples as *decapped*.

As discussed below, after decapping we observe a Bi-rich phase at the surface of $GaAs_{1-x}Bi_x$, with $x > 0$. Since we are particularly interested in the bulk properties we treated GaAsBi samples by a short ion bombardment (Ar^+ pressure 1×10^{-6} mbar, ion energy 1 keV, and sputtering times between 1 min and 12 min) and subsequent annealing to 400–440° C. We will refer to these samples as *sputter-annealed*. Typical LEED images of *sputter-annealed* GaAsBi samples are shown in Fig. 1(b). A (2 × 3) pattern is evident. *Sputter-annealed* GaAsBi surfaces exhibit sharper LEED patterns than the *decapped* surfaces.

XPS and *k*-PEEM measurements were carried out using an *Omicron NanoESCA* instrument with laboratory light sources. The *NanoESCA* photoemission spectrometer is based on a PEEM column and an imaging double hemispherical energy filter [7] with an energy resolution of $\Delta E = 0.1$ eV. A transfer lens in the electron optics switches between the real space and angle-resolved *k*-PEEM modes, which allows to perform classical XPS with monochromatized Al $K\alpha$ radiation, as well as an energy dependent mapping of the Brillouin zone (BZ) using a helium discharge lamp at $h\nu = 21.2$ eV. Highly resolved XPS and UPS data were measured independently at the ELETTRA synchrotron radiation facility (*Materials Science Beamline*) with predominantly linearly polarized light in the horizontal direction.

In semiconductors the position of the Fermi energy (E_F) with respect to the valence band maximum (VBM) is sensitive to defect states and possible surface band bending effects. We expect Bi atoms in GaAs to cause shifts of E_F, which in turn will affect binding energy (BE) values detected in photoemission experiments. Kraut *et al.* [8] described procedures to quantify defect induced shifts in E_F and band bending in GaAs by referencing shallow core level (CL) binding energies such as $E_{Ga\,3d}$ to the VBM value E_{VBM}. Throughout this work we follow Kraut *et al.* and estimate values of E_{VBM} using the leading edge method, which approximates the density of states (DOS) by a tangential line at the maximum steepness of the VB edge. Figure 2 shows an example of photon energies $h\nu = 1.5$ keV. Values E_{VBM} derived from XPS, *k*-PEEM, and UPS data in this work are listed in Table I. In the case of pure GaAs(001) ($x = 0\%$) average values are (0.75 ± 0.1) eV, which correspond to Fermi level pinning close to the middle of the band gap typical for *n*-type MBE-grown GaAs [9].

B. Theoretical simulations

Geometry and electronic structure calculations were carried out using density functional theory (DFT) within the local density approximation (LDA) as implemented in the QUANTUM ESPRESSO code [10]. Spin-orbit coupling (SOC) was accounted for by means of fully relativistic ultrasoft pseudopotentials [11], including nonlinear core corrections

TABLE I. Overview of VBM energy values E_{VBM} derived from XPS, UPS, and *k*-PEEM data, shown in Fig. 2, Fig. 6, and Fig. 10, respectively. Values for finite Bi concentrations correspond to the *sputter-annealed* state. All values were extracted using the leading edge method and error bars are estimated to be 0.05 eV.

Bi content x	0 %	0.8 %	2.7 %
XPS [eV]	0.83	–	0.42
k-PEEM [eV]	0.68	0.50	0.55
UPS [eV]	0.75	0.35	0.34

for all species and semicore d states in the valence for both Ga and Bi [12]. The kinetic energy cutoff was 30 Ry (300 Ry for the charge), and the theoretical lattice constant of 5.61 Å was adopted. Structural relaxations used a threshold of 5 meV/Å. As shown in Appendix B, our LDA + SOC scheme adequately describes the occupied bands of GaAs that lie within 5 eV of the valence band maximum. It furthermore predicts lattice constants for GaAs (and GaBi) accurate to 0.05 Å of the (estimated) experimental values. On the other hand, LDA considerably underestimates the electronic band gap of GaAs by over 1 eV. For this reason our work is focused on the occupied band structure.

Two types of system were considered. First, a 128-atom $4 \times 4 \times 4$ supercell was used to compute the electronic structure of bulk GaAs and GaAsBi. In the latter, Bi was substituted for As at densities of 1.6% and 3.2% (1 and 2 Bi atoms per cell, respectively), and all atoms were allowed to relax. Γ-centred $(2 \times 2 \times 2)$ k-point meshes were used. Second, the GaAs(001)-$\beta 2(2 \times 4)$ surface reconstruction was studied using a supercell geometry. Thin GaAs slabs containing ten atomic layers (14 Å thick) were separated from their periodic replicas by 20 Å. Γ-centred $(4 \times 8 \times 1)$ k-point meshes were used during structural relaxations. The As-terminated back surface was fixed to bulk positions and passivated with pseudohydrogen. As shown in Sec. III, Bi is mostly present in the bulk layers of the *sputter-annealed* surface. We therefore consider the effect of Bi substitution only in the central bulk layers of the 2×4 reconstructed slab. Thus we do not consider the measured 2×3 periodicity of the GaAsBi surface nor the possible influence of Bi on surface states. Note that the precise 2×3 structure is anyway difficult to ascertain, being a mixture of 4×3 phases possibly featuring Bi-As or Bi-Bi dimers on the surface [13].

The computed electronic properties were analyzed through different techniques. First, the band structures of the bulk $4 \times 4 \times 4$ and slab 2×4 supercells were unfolded along high symmetry directions in the primitive bulk GaAs BZ and 1×1 surface BZ (SBZ), respectively, using the BANDUP code [14,15]. This allowed us to make a direct comparison to k-PEEM data and helps to decouple surface and Bi-related states from bulk states of GaAs. Second, the integrated density of states (DOS) and k-resolved DOS of the 2×4 slab and of bulk GaAs were computed. In the slab case, the DOS was further projected onto surface and bulk atomic orbitals, respectively, in which the surface is defined as including all dimers and backbonds (layers 1–4), and the bulk makes up the remainder (layers 5–10). The k-resolved DOS was computed along various high symmetry lines as a function of energy and also as constant energy cuts [two-dimensional (2D) maps] through the full reduced zone SBZ.

III. X-RAY PHOTOEMISSION SPECTROSCOPY

Figure 2 shows photoemission data of GaAs(001)-(2×4) at low BEs in comparison with data for decapped GaAsBi. The high photon energies of $h\nu = 1.5$ keV correspond to a probing depth of several nanometers and thus the data mainly reflect bulk properties. In the case of pristine GaAs(001)-(2×4) we derive a value of $E_{\rm VBM}^{\rm GaAs} = (0.83 \pm 0.05)$ eV using the leading edge method as described in Sec. II A. The

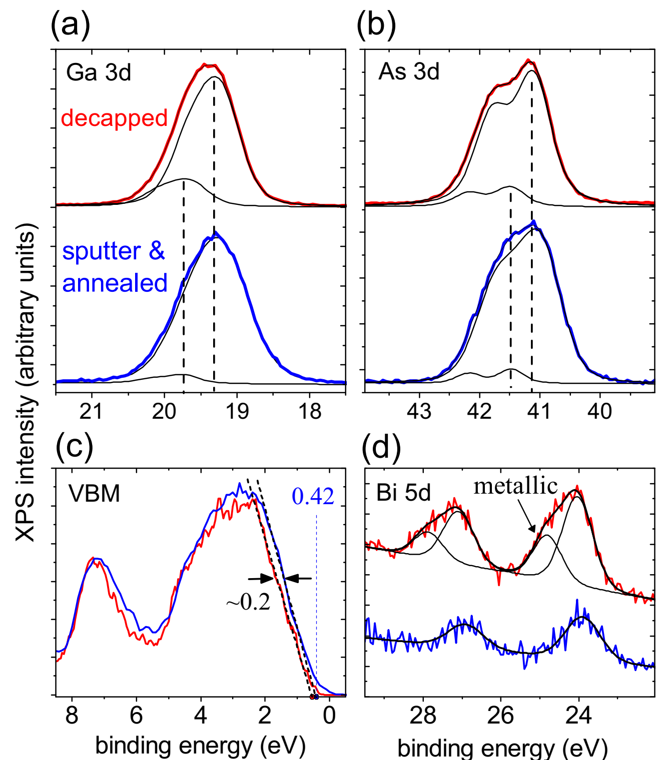

FIG. 3. Sputtering and annealing effects on (a) Ga 3d, (b) As 3d, (d) Bi 5d core levels, as well as on (c) valence band spectra measured at 1.5 keV. $GaAs_{1-x}Bi_x$ ($x = 2.7\%$) is shown in its *decapped* (red) and *sputter-annealed* state (blue). The value $E_{\rm VBM}^{\rm GaAsBi} = 0.42$ eV in the *sputter-annealed* state is derived using the leading edge method indicated by the tangential dashed lines in (c).

relative BE of the Ga 3d level with respect to the VBM then amounts to $(E_{\rm Ga\,3d}^{\rm GaAs} - E_{\rm VBM}^{\rm GaAs}) = (18.82 \pm 0.05)$ eV, which is in good agreement with the bulk value of 18.80 eV reported on GaAs(110) [8]. Comparing $E_{\rm VBM}$ of GaAs to *decapped* GaAsBi ($x = 2.7\%$), a shift to lower BEs is visible in Fig. 2, which we estimate as $(E_{\rm VBM}^{\rm GaAs} - E_{\rm VBM}^{\rm GaAsBi}) = (0.23 \pm 0.05)$ eV. The origin of such shifts can be Bi-induced defect levels in the gap or changes in band bending. At the same time BE values of $E_{\rm Ga\,3d}^{\rm GaAsBi}$ shift by about the same amount. Taking into account the limited energy resolution of the laboratory *NanoESCA* instrument we estimate Bi-induced changes in the relative Ga 3d CL positions $(E_{\rm Ga\,3d} - E_{\rm VBM})$ to be smaller than 0.1 eV.

Short sputtering treatments (described in Sec. II A) create near-surface defects. However, under the influence of subsequent annealing cycles at temperatures of 400–440° C, the surfaces reorder into 2×3 symmetries. Figure 3 summarizes respective changes in the XPS data. Within the energy resolution of our XPS setup Ga 3d and As 3d CL spectral shapes, shown in Figs. 3(a) and 3(b) always contain at least two components, which we attribute to a dominating bulk signal and additional chemically shifted surface components both for Ga and As. Respective fits assuming one single surface component are added to the XPS data in Figs. 3(a) and 3(b). In the *sputter-annealed* state Ga 3d and As 3d CLs are broadened, evidencing an enhanced disorder of the host structure. Again,

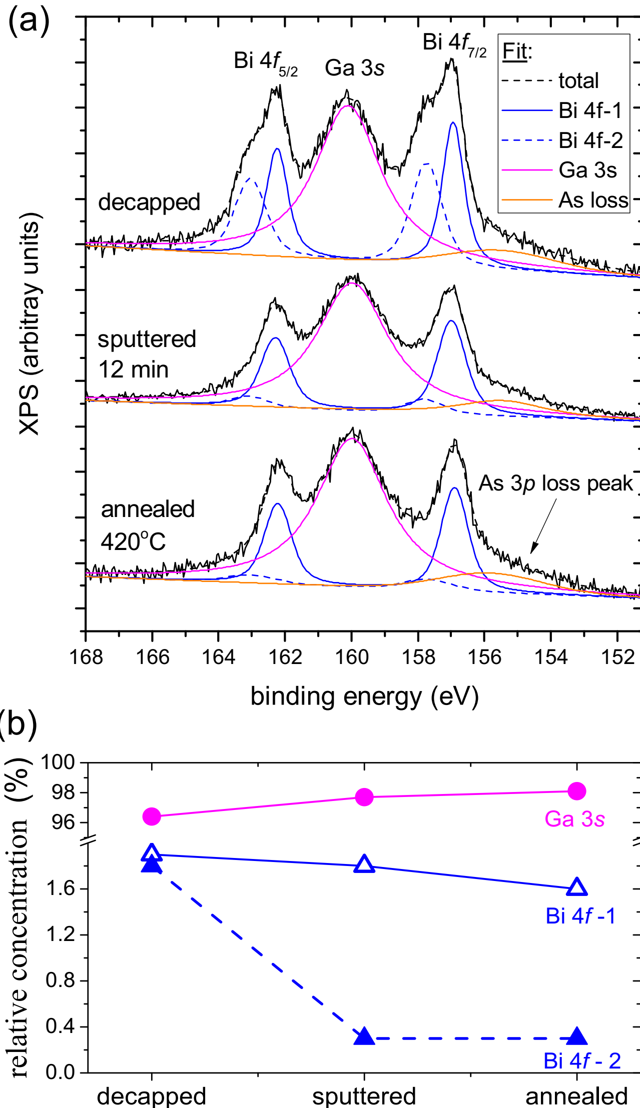

FIG. 4. (a) Bi 4f XPS spectra of $GaAs_{1-x}Bi_x$ ($x = 2.7\%$) after decapping, subsequent 12 min sputtering, and final annealing at 420°C (top to bottom). The fit shown to the data consists of one Ga 3s line and two Bi 4f doublets denoted as Bi 4f-1 and Bi 4f-2. A broad loss peak is present at about 155 eV, which originates from the As 3p edges at lower BEs. Fit parameters are listed in Table II and described in Appendix A. In (b) the respective relative atomic concentrations of Bi and Ga components are plotted for the three sample stages.

we reference CLs to E_{VBM}, which is shown in Fig. 3(c) for GaAsBi ($x = 2.7\%$). During sputtering-annealing treatment the VBM moves by 0.2 eV towards lower values. In the case of Bi 5d CLs a more significant change in spectral shape is visible after sputtering and annealing, which goes beyond a simple broadening effect and corresponds to the suppression of a higher BE component at about 25 eV typical for a metallic coordination between Bi atoms. This interpretation is backed by data on Bi 4f CLs, as we discuss in the following.

In the initial *decapped* surface, shown at the top of Fig. 4(a), the Bi 4f XPS signal can be decomposed into two Bi doublets with the main $4f_{7/2}$ peaks located at BEs of (157.0 ± 0.1) eV and (157.7 ± 0.1) eV, which we denote as Bi 4f-1 and Bi 4f-2 hereafter. The fit was derived using the KOLXPD program as described in Appendix A and respective fit parameters are given in Table II. The Bi 4f-2 BE position (157.7 ± 0.1) eV is close to literature values attributed to a Bi metallic state [16]. Twelve minutes of argon sputtering almost completely removes the metallic Bi 4f-2 component (see middle panel), while Bi 4f-1 and Ga 3s components remain stable although slightly broadened. Integrated XPS intensities of respective components can be converted into relative atomic concentrations (see detailed description in the Appendix A), which are plotted in Fig. 4(b). The low concentrations of 4f-2 after sputtering proves the near-surface character of the metallic phase, which is further supported by the fact that no strong differences in Bi XPS spectral shapes were observed when sputtering times were reduced from 12 min to 1 min. On the contrary, we identify the stable Bi 4f-1 component at (157.0 ± 0.1) eV with bulk-incorporated Bi atoms in the host GaAs lattice, most likely Bi_{As} substitutional sites, as suggested by Sales *et al.* [6]. Bulk Bi concentrations in Fig. 4(b) of $x \approx 2\%$ are slightly lower than nominal values of $x = 2.7\%$.

Finally, Fig. 4(a) (lower set of curves) shows that annealing procedures up to 420° C after sputtering does not trigger a reappearance of the metallic Bi phase in XPS. It proves the absence of major diffusion processes of Bi atoms at temperatures used throughout this work.

TABLE II. KOLXPD fitting parameters of Ga 3s, and Bi 4f XPS spectra shown in Fig. 4(a). BEs of Bi 4f refer to the main $f_{7/2}$ peak. Details on the fitting procedure are described in Appendix A.

	Bi 4f-1	Bi 4f-2	Ga 3s	As loss
Annealed				
BE [eV]	156.94	157.74	160.1	155.52
Concentration [%]	1.9	1.8	96.3	–
Sputtered				
BE [eV]	156.99	157.79	159.97	155.47
Concentration [%]	1.8	0.3	97.9	–
Annealed				
BE [eV]	156.90	157.70	159.99	155.82
Concentration [%]	1.6	0.3	98.1	–

IV. ANGLE-RESOLVED k–PEEM STUDIES

A. GaAs(001)

A prerequisite for momentum resolved k-PEEM measurements is a sufficient crystalline surface order of the samples under study, which we achieve even for finite Bi concentrations, as described in Sec. II. We first discuss the case of GaAs without Bi. After decapping pure GaAs(001) (0% Bi) surfaces we observe the well-known (2 × 4) reconstruction, as shown in Fig. 1(a). Its electronic [17–20] and optical [21,22] properties have been deeply studied within the past decades. The geometry is the well-known $\beta2(2 \times 4)$ reconstruction, containing two As dimers in the first layer and a third As dimer in the third layer [23]. The corresponding (2 × 4) SBZ is shown in Figs. 5(a) and 5(b) relative to that of the (1 × 1) SBZ. In the following, special point labels of the (2 × 4) SBZ

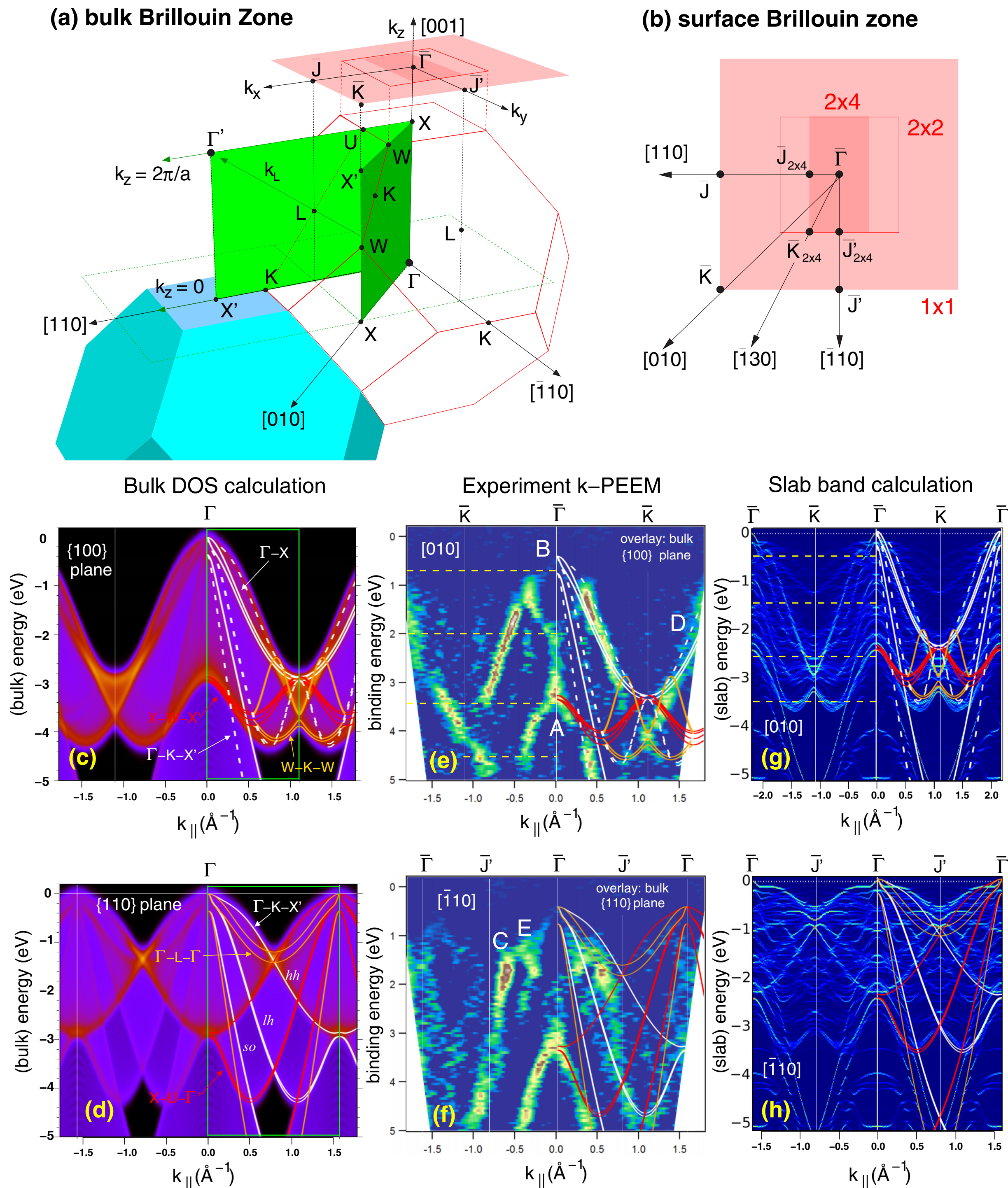

FIG. 5. (a) Bulk and (b) surface Brillouin zones (BZ) of GaAs(001). Bulk high-symmetry points outside the first BZ have a prime symbol (Γ′, X′). (c) Bulk GaAs DOS plotted along [010] and averaged over k_z, corresponding to the dark-green plane ΓXX′X shown in (a). (d) As (c), for the [110] direction and the light-green plane ΓX′Γ′X. Selected bands along high symmetry lines lying in these planes and projected onto $k_\parallel$ are overlaid on the right-hand side of each panel. (e, f) Experimental k-PEEM data for [010] and [$\bar{1}$10] directions, with computed bulk bands overlaid as in (c, d). (g, h) Unfolded slab band structures for the $\beta 2(2 \times 4)$ reconstruction for the [010] and [$\bar{1}$10] directions. Bulk overlays are compressed to match the slab bands. Horizontal dashed lines in (e) and (g) indicate energies at which (k_x, k_y) distributions shown in Fig. 8 are generated. Computed energies are shown with respect to the VBM, experimental energies with respect to the measured Fermi level.

are indicated by an explicit subscript; otherwise, points refer to the (1×1) SBZ.

Experimental k-PEEM data for photon energies $h\nu = 21.2$ eV are shown in Figs. 5(e) and 5(f) for $k_\parallel$ along the [010] ($\bar{\Gamma}$–$\bar{\mathrm{K}}$) and [$\bar{1}$10] ($\bar{\Gamma}$–$\bar{\mathrm{J}}'$) directions, respectively. The data cover a range of $k_\parallel = \pm 1.8$ Å^{-1}, centered at $\bar{\Gamma}$, and BEs are given with respect to E_{F} of the k-PEEM analyzer. Again, we estimate E_{VBM} at $x = 0\%$ using the leading edge

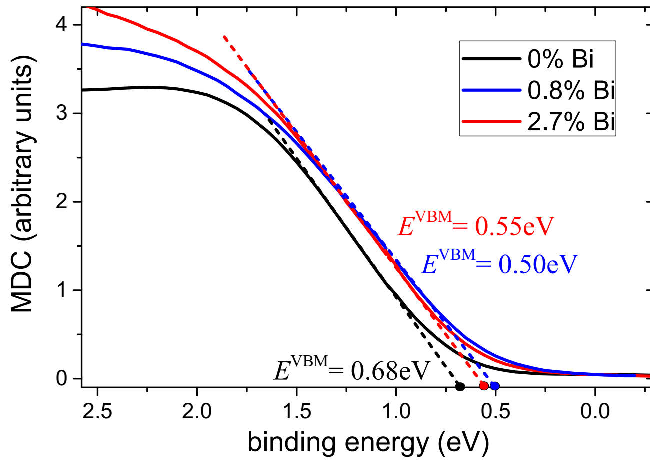

FIG. 6. Momentum integrated k-space intensity close to the VBM plotted vs energy. The photon energy is $h\nu = 21.2$ eV. Dotted lines show the estimation of the VBM according to the leading edge method.

method, as shown in Fig. 6, based on k-space integrated intensities. We derive a value of $E_{VBM}^{GaAs} = (0.68 \pm 0.05)$ eV, which is close to the value from XPS data (see also Table I), although the probing depth of measurements at $h\nu = 21.2$ eV is significantly lower than in the XPS mode. We infer that band bending effects do not significantly affect the values of E_{VBM}^{GaAs}. Typical screening lengths of MBE-grown GaAs are 1–2 nm. Both cuts in Figs. 5(e) and 5(f) show similar band structures with several common features that are marked *A*-*E* (partly following the notation of Souma *et al.* [24]), although the [010] cut appears somewhat narrower at lower BEs. Band *B* shows a maximum at Γ and continuously disperses down to BE = 3.5 eV. A characteristic "wishbone" feature *A* is observed below 3.2 eV at $\bar{\Gamma}$.

At these incident energies we expect a dominant contribution from bulk states, and thus associate the maximum at $\bar{\Gamma}$ with the peak in the light-hole (*lh*) or split-off (*so*) band of bulk GaAs. To understand the data further, one must consider the relation between the (1 × 1) SBZ and the bulk GaAs BZ, as depicted in Fig. 5(a). During k-PEEM, as in ARPES, the momentum k_z perpendicular to the surface is not conserved. To interpret the measured data along some $k_\parallel$, one should thus consider a suitable average over k_z [25]. For instance, a measurement along [010] ($\bar{\Gamma}$–$\bar{\text{K}}$) will probe all ($k_\parallel$, k_z) in the ΓXX′X plane [see dark-green plane in Fig. 5(a)].

As a first approximation of the k-PEEM data, we computed within DFT (including spin-orbit coupling) the DOS of bulk GaAs resolved on a (100 × 40) grid of $k_\parallel$, k_z points along the [010] and [110] directions, before taking a simple average over k_z for each value of $k_\parallel$. The results are plotted as colormaps in Figs. 5(c) and 5(d), and extended across the measured range of $k_\parallel$. Overlaid on these maps are the computed bulk bands along selected high-symmetry lines. It appears that most of the $k_\parallel$-resolved DOS can be well represented by a handful of selected bands passing through the high-symmetry points of the bulk BZ [24,25].

To facilitate a better comparison to experiment, these selected bands are also overlaid on the k-PEEM data in Figs. 5(e) and 5(f). The $k_\parallel$-resolved DOS clearly succeeds in explaining most of the observed signal. Feature *A* at $\bar{\Gamma}$ arises from the contributions at $k_z = 2\pi/a$, i.e., the lines X-W-X′ and X-U-Γ′ drawn in red. We stress that *A* can only be explained by considering the k_z dependence [24]. The intense signal spreading out symmetrically below *A* is explained first by the dispersion of the $k_z = 2\pi/a$ lines and then, for higher BEs, by the diagonal projections Γ-K-X′ [in Fig. 5(c)] and Γ-L-Γ′ [in Fig. 5(d)]. The intense vertical line above *A* (BE = 2.0–3.4 eV) in the [010] case instead cannot be associated with a single band, but corresponds well to a region of high DOS visible only in the $k_\parallel$-resolved map [Fig. 5(c)]. Features *C* and *D* are well explained by heavy-hole (*hh*) or light-hole (*lh*) bands arising from the $k_z = 0$ lines. Note that the horizontal signal "widths" for both directions are determined by the Γ-K-X′ line. However, its contribution is projected onto $k_\parallel$ for the [010] case, resulting in the overall narrower lineshape observed experimentally.

Good agreement with experiment is also obtained for the DFT band structure of the full GaAs(001)-β2(2 × 4) slab, plotted in Figs. 5(g) and 5(h) and unfolded across the full (1 × 1) BZ. Due to the use of a relatively thin slab, any extended (bulk-like) wave functions undergo size quantization and thus the computed band structure is compressed relative to the bulk GaAs case. This is illustrated by overlaying and compressing the selected bulk bands until a reasonable match is reached (see Fig. 5). Note that the slab bands naturally include the k_z averaging procedure as the three-dimensional (3D) BZ of the large (slab plus vacuum) supercell is significantly compressed. In addition to the dispersive bulk bands, several reconstruction-related features become apparent. A dispersive band with minimum around 1.1 eV at $\bar{\text{K}}$ is visible along [010], while flatter features appear in the 0.8–1.2 eV range along [$\bar{1}$10]. This last in particular is suggestive of surface states.

In the 2 × 4 reconstruction the bulk symmetry between [110] and [$\bar{1}$10] directions is broken and respective surface electronic properties should differ. Figure 7 adds k-PEEM data also for the [110] and [$\bar{1}$30] directions. Note that signals from $\bar{\Gamma}$ in the second SBZ are visible in both Figs. 7(b) [110] and 7(c) [$\bar{1}$10] data. Both cuts show very similar band structures, consistent with our explanations of the main features as arising from the bulk DOS averaged in the (110) plane. The "wishbone" feature in the [110] data is now more clearly shown to be derived from two distinct bands that cross at around 3.7 eV. Band *B* is observed in all four cuts.

Further confirmation of the origin of these bands is obtained by performing constant energy cuts of the k-PEEM data. Exemplary energy cuts at BE = 0.75, 2.0, 3.4, and 4.5 eV [indicated by horizontal dashed lines in Fig. 5(e)] are shown in Figs. 8(a) to 8(d). They confirm asymmetries between the [110] and [$\bar{1}$10] directions. The measurements are in generally good agreement with appropriate energy cuts [see lines in Fig. 5(g)] through the unfolded slab band structures, as reported in Figs. 8(e) to 8(h). It is worth noting that in the energy cut at BE = 0.75 eV in Fig. 8 the (k_x, k_y) intensity reveals a cloverleaf structure which is elongated along the [$\bar{1}$10] direction with respect to [110]. This pattern is also evident in the (k_x, k_y)-resolved DOS at 0.55 eV of the (folded) (2 × 4) slab, shown as an inset in Fig. 8(e). The bulk GaAs

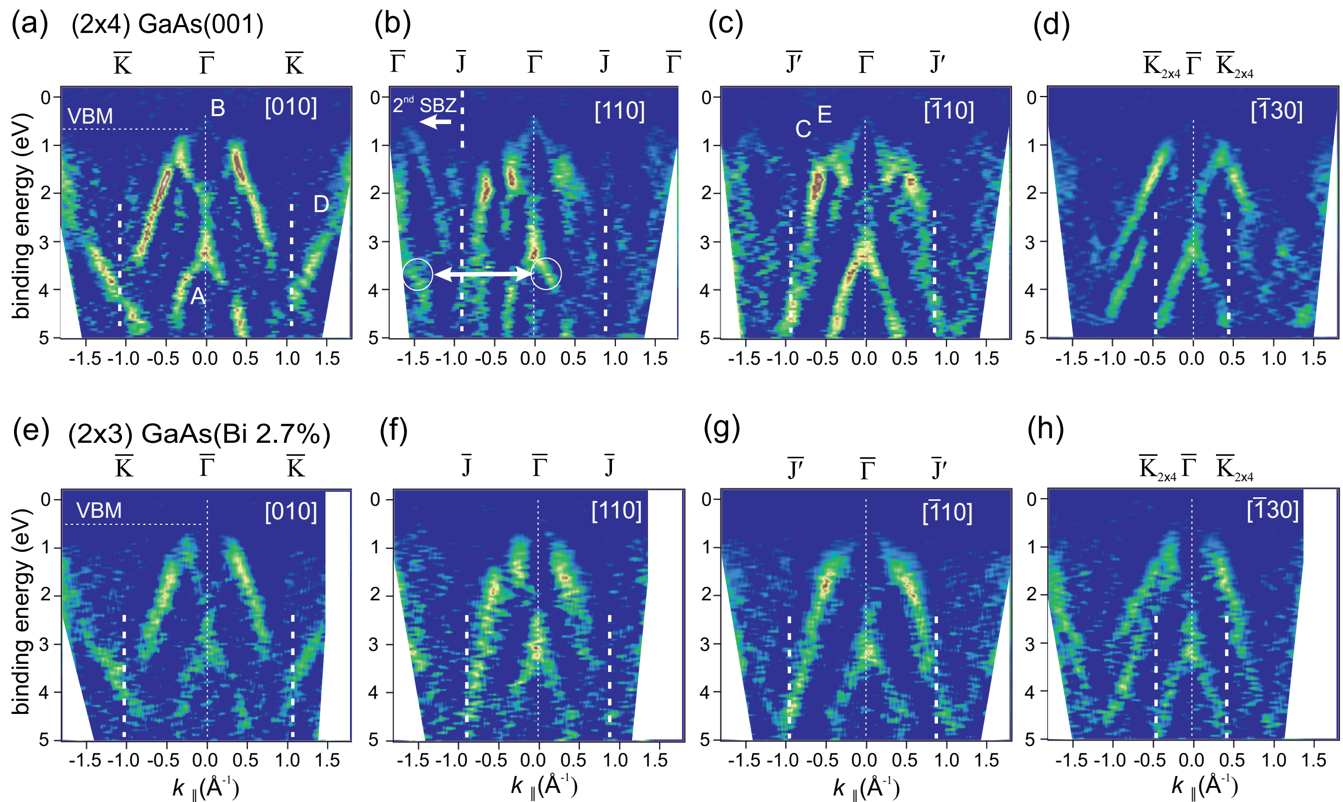

FIG. 7. *k*-PEEM comparison of *decapped* (2×4) GaAs(001) (top row) and *sputter-annealed* (2×3) GaAsBi (bottom row). Respectively, (a)–(d) and (e)–(h) correspond to cuts along the $\bar{\Gamma}$–$\bar{K}$, $\bar{\Gamma}$–$\bar{J}$, $\bar{\Gamma}$–$\bar{J}'$, and $\bar{\Gamma}$–$\bar{K}_{2\times4}$ directions. Horizontal dashed lines indicate E_{VBM} values derived from Fig. 6. The horizontal arrow in (b) indicates the replica of feature *A* in the second SBZ at the expected distance $\Delta k = 1.56$ Å^{-1}.

electronic structure close to VBM is known to have As 4*p* character with four-fold cubic symmetry in the bulk, while for GaAs 2×4 surfaces we expect a symmetry breaking. Band *C* is assigned to the light-hole bands supported by the rather spherical shape in the (k_x, k_y) distribution at BE = 2.0 eV [see cut shown in Fig. 8(b)]. Heavy hole bands on the other hand were found to become visible only at higher photon energies as shown by Kanski *et al.* [26].

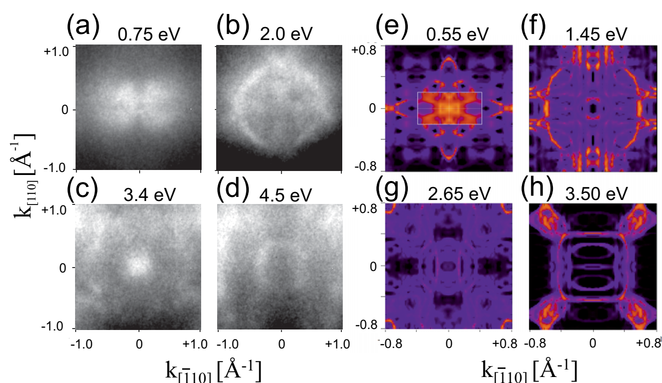

FIG. 8. Left: Constant energy cuts of pristine GaAs(001) *k*-PEEM data. Intensity distributions (k_x, k_y) are shown at four BEs (a) 0.75 eV, (b) 2.0 eV, (c) 3.4 eV, and (d) 4.5 eV. Right: band structure maps of the GaAs(001)-$\beta2(2 \times 4)$ slab, computed at the constant energies indicated in Fig. 5(g), and unfolded across the (1×1) SBZ. Panel (e) inset shows the (k_x, k_y)-resolved DOS of the (2×4) SBZ. Theoretical energies in (e)–(h) are referenced to the VBM, while experimental data (a)–(d) are given with respect to the Fermi level.

In addition to the above bulk-derived features, we also identify an additional feature *E* in Fig. 5(f) which crosses *B* at BE = 1.8 eV and $k = \pm 0.4$ Å^{-1}, reminiscent of a backfolding effect to the first BZ. This feature is missing from the bulk DOS calculations, and has not been reported in previous literature [24]. It may be consistent with the aforementioned feature at -1 eV in the slab band calculations in Fig. 5(g) that are suggestive of surface state origin.

B. GaAs(001) with Bi

We now turn to the effect of Bi incorporation on the GaAs band structure. Figure 7 (bottom row) summarizes *k*-PEEM data of *sputter-annealed* $\mathrm{GaAs_{1-x}Bi_x}$ ($x = 2.7\%$) in comparison to *decapped* GaAs(0% Bi) (top row) for high-symmetry directions $\bar{\Gamma}$–$\bar{K}$, $\bar{\Gamma}$–$\bar{J}$, $\bar{\Gamma}$–$\bar{J}'$, and $\bar{\Gamma}$–$\bar{K}_{2\times4}$. The respective 2×3 and 2×4 LEED symmetries were shown in Figs. 1(a) and 1(b) and previously discussed in Sec. II.

Rigid shifts of the *k*-PEEM band structures of GaAsBi to lower BEs with respect to pure GaAs confirms our XPS observations. Figure 6 shows reduced values for $E_{\mathrm{VBM}}^{\mathrm{GaAsBi}}$ of (0.50 ± 0.05) eV and (0.55 ± 0.05) eV for Bi concentrations $x = 0.8\%$ and $x = 2.7\%$, respectively (see also Table I). If we assume that band bending is negligible, the shift of the VBM

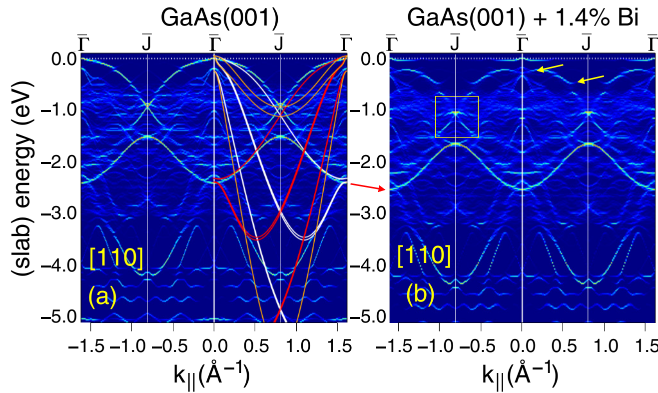

FIG. 9. Band structure of GaAs(001)-$\beta 2(2 \times 4)$ slab unfolded along [110]: (a) pristine (2×4) cell and (b) including 1 atom of Bi in a (4×4) supercell.

to lower BEs suggests the formation of shallow p-type defect states, which would pin E_F closer to the VBM.

The shift in the VBM is accompanied by a general broadening of k-PEEM features compared to pure GaAs despite the well-defined LEED pattern in Fig. 1(b). In particular, along the $\bar{\Gamma}$–$\bar{\text{K}}$ and $\bar{\Gamma}$–$\bar{\text{K}}_{2\times4}$ directions the band structure of GaAsBi appears to match that of GaAs but is considerably broadened. Looking closer, the feature E along the $\bar{\Gamma}$–$\bar{\text{J}}'$ direction is particularly affected [see Fig. 7(f)], which seems to have entirely disappeared. It points towards surface related broadening of the feature E. Thus, it would confirm the above discussed interpretation of our 2×4 GaAs slab calculations in the direction of a surface state origin of feature E.

Slab calculations incorporating Bi in a bulk site succeed in reproducing the main observed experimental features. Figure 9 compares the pristine $\beta 2(2 \times 4)$ slab band structure unfolded along [110] to that of a slab containing a low concentration of Bi. The main effect of Bi is to perturb the bands coming from bulk GaAs, in particular the heavy hole band (yellow arrows). At the Γ point, the VBM almost appears detached from the rest of the *hh* band along this direction, such that it resembles a new defect level. Such defects could explain shifts of the VBM to lower BEs observed in k-PEEM experiments. Other points in the SBZ also lose their clear Bloch character (see box at $\bar{\text{J}}$). A small shift or change in the bandwidth is also observed (red arrow). However, due to the dense manifold of bulk and surface bands in these supercells it is difficult to make any quantitative analyses: this is discussed instead in the following section.

V. ULTRAVIOLET PHOTOELECTRON SPECTROSCOPY STUDIES

The k-PEEM measurements reported in the previous section succeed in identifying mainly bulk-derived electronic states in GaAs and GaAsBi. However, the limited resolution makes it difficult to identify surface related features previously identified, for instance, with ARPES [20]. To examine the surface electronic structure in more detail we measured UPS in a highly resolved mode at the ELETTRA synchrotron facilities. In particular, the possibility to vary the photon energy at the synchrotron allows to probe the dimensionality of surface states. True surface states do not disperse with photon energy due to their strict 2D nature. On the other hand, for surface resonances a strong hybridization with the 3D bulk band structure allows dispersive effects to occur.

Figures 10 and 11 show UPS data in normal emission taken at selected photon energies between 25 and 100 eV. Bi containing samples were measured in the *sputter-annealed* state. At high BEs > 3 eV the spectra of all samples are dominated by two weakly dispersive features at 7.6 and 12.3 eV shown in Fig. 11 (labeled d and e) and one strongly dispersing band c which joins d at a photon energy of 40 eV. In addition pure GaAs shows a prominent almost nondispersing band b at 4.2 eV, which is strongly suppressed for $x = 0.8\%$ Bi and fully disappears at $x = 2.7\%$ Bi.

Spectra taken from *decapped* GaAs(001) are in good agreement with the literature, e.g., for GaAs(001)-(2×4) at $h\nu = 29$ eV [20]. According to the literature the bands c and d are primary cone bulk emission peaks and can be attributed to direct interband transitions from bulk valence bands to a free-electron-like final state. The dispersive behavior of the bands versus photon energy is plotted in Fig. 12(a). We referenced the band dispersion to the relevant VBM value $E_{\text{VBM}}^{\text{GaAs}} = 0.75$ eV derived in Fig. 10 using the leading edge method (see also Table I). Band c shows strong dispersion and a shallow minimum at 43 eV, while d is flat.

Both findings coincide very well with those of Cai *et al.* [17] on GaAs(001)-(1×1), confirming that a and d are independent of the particular surface reconstruction as expected for bulk bands. The minimum of c at a photon energy of about 44 eV corresponds to the X_6 point in $k_\perp$ along the $\Gamma\Delta X$ direction [see label in Fig. 12(a)] and is attributed to the split-off band. Close to the VBM the UPS data of pure GaAs show two features a_1 and a_2, which join at low photon energies $\leqslant 23$ eV to form one single band a [see label in Fig. 12(a)]. Again this is in good agreement with Cai *et al.* and suggests that a_2 corresponds most likely to the *hh* and *lh* band excitation.

Figure 12(b) shows the band dispersions of GaAsBi samples with 0.8% and 2.7% Bi concentrations. Data of pure GaAs from Fig. 12(a) is replotted as continuous lines for direct comparison. Comparing the two GaAsBi samples it is striking that the two datasets at 0.8% and 2.7% Bi mostly coincide. The respective VBM values for GaAsBi samples are also similar with $E_{\text{VBM}}^{\text{GaAsBi}} = 0.35$ eV $(x = 0.8\%)$ and $E_{\text{VBM}}^{\text{GaAsBi}} = 0.34$ eV $(x = 2.7\%)$, shown in Fig. 10. For a comparison with previous values see also Table I. In comparison to pure (2×4) GaAs(001), however, significant differences are visible. The (a_1, a_2) bands closer to the VBM are broadened and cannot be distinguished anymore, as shown on a larger scale in Fig. 10. We therefore label them henceforth as a. The dispersion of a comes to lie between a_1 and a_2 and suggests minor shifts in the *hh* and *lh* bands under the influence of Bi, although the general broadening limits the certainty of this statement. On the other hand, bands c and d are clearly shifted to higher BEs for Bi-containing samples. The shift in c amounts to about +0.4 eV, while d shifts by +0.2 eV.

So far we neglected surface states (SSs), which contribute to the DOS close to the VBM and should be most affected by reconstruction effects. It is known from the literature on various GaAs surfaces that shallow SSs become visible as typical

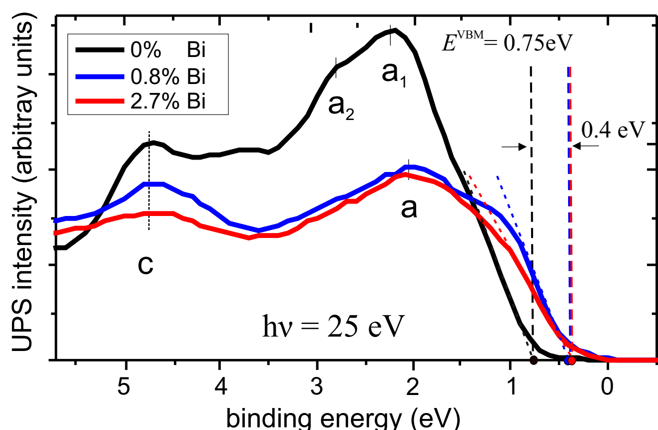

FIG. 10. Normal emission UPS close to the VBM for Bi concentrations 0%, 0.8%, and 2.7%. The photon energy is $h\nu = 25$ eV. Values for $E_{\rm VBM}$ were derived using the leading edge method as shown by vertical lines in the plot.

shoulders [17,19] in the UPS intensity close to the VBM. In Fig. 11(a) such a shoulder is labeled SS as an example which is clearly separated from the intensities a_1 and a_2 especially at low photon energies. The introduction of Bi in the GaAs matrix affects the valence band lineshape, and this distinction in Fig. 10 is less pronounced. Upon Bi incorporation the SS shoulder partly overlaps with the broadened contribution a and is shifted to lower BEs. Although incorporation of Bi in the GaAs(001) slab calculations does yield tangible changes [see Fig. 9(b)], the strong folding makes it difficult to determine the precise influence of Bi-incorporation on specific bulk bands. We thus performed supercell calculations of *bulk* GaAs and a basic analysis of Bi incorporation on the bulk electronic properties, similar to the study of Bannow *et al.* [27].

Figure 13 demonstrates the influence of Bi incorporation for 1 and 2 Bi atoms per 128-atom $4 \times 4 \times 4$ supercell, consistent with concentrations of 1.56% and 3.12% Bi, respectively. Figure 13(a) reports the folded (reduced zone) band structures within 1 eV of the gap in each case. Only one Bi–Bi configuration is illustrated for the 3.12% Bi case, in which the Bi atoms are 4Å apart and aligned along the [110] direction. As discussed later, this configuration causes relatively strong perturbations to the GaAs electronic structure. All bands are plotted with respect to the VBM of pure GaAs, following an appropriate alignment of the average electrostatic potential. The contribution of Bi orbitals to each state is proportional to the size of the black dots overlaid on the bands. Note that the bottom of the conduction band is also indicated: the band gap is greatly underestimated, as expected in LDA (see Appendix B). Figure 13(b) shows wave functions of selected bands at the Γ point as cuts on the $(1\bar{1}1)$ plane that intersects the Bi atom positions. The corresponding (E, k) points are indicated in Fig. 13(a) by open circles. The corresponding unfolded band structures (extended zone scheme) are shown in Figs. 13(c) and 13(d). Bands are plotted over a wider energy range and aligned to the VBM of each system to compare directly to the experimental data in Fig. 12.

These calculations demonstrate a number of trends for increasing Bi concentrations. (i) Bi induces significant perturbations on the hh and lh bands near the VBM. At the Γ point, the Bi-orbital contribution increases from 5% to 15% (hh band) or 8% (lh band), and a clear splitting is observed at the higher concentration. This is somewhat consistent with the observed behavior of a_2 in Fig. 12(b) at low photon energies. (ii) Away from Γ, degeneracies occur at the zone boundaries in the folded band scheme that manifest in the unfolded

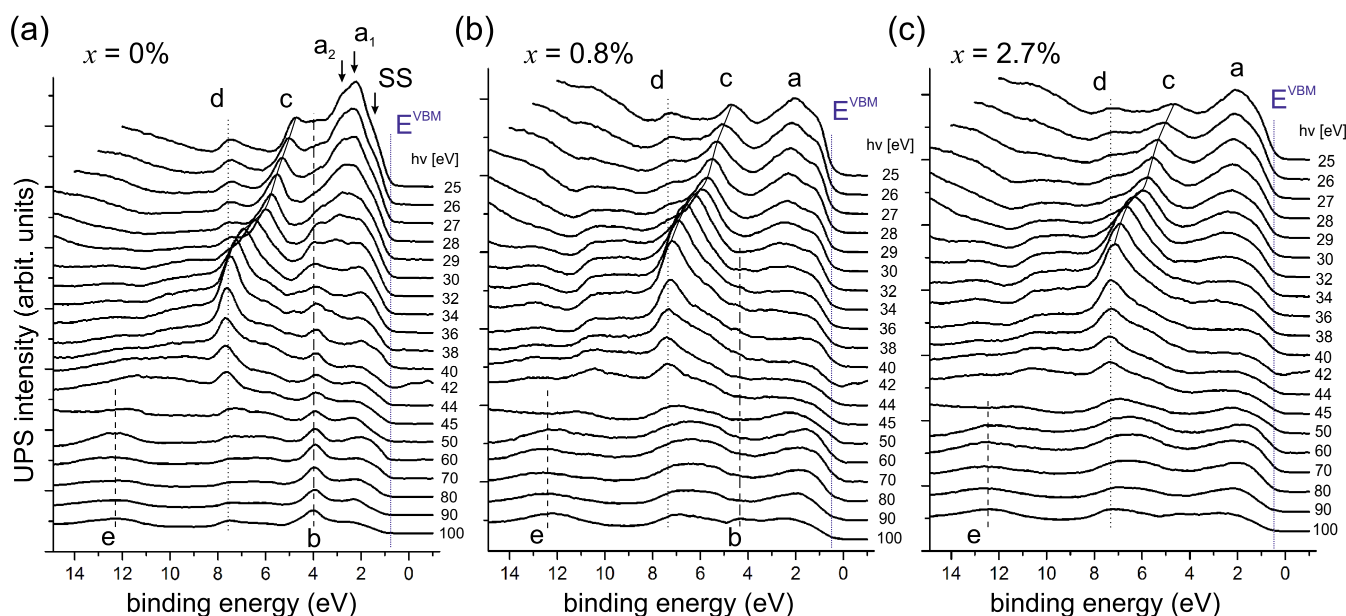

FIG. 11. Photon energy dependent normal emission UPS spectra for 0%, 0.8%, and 2.7% Bi concentrations (a)–(c), respectively. Samples are in the *sputter-annealed* state. Features indicated by *a*–*e* are explained in the text. Vertical blue lines correspond to $E_{\rm VBM}$ values derived in Fig. 10.

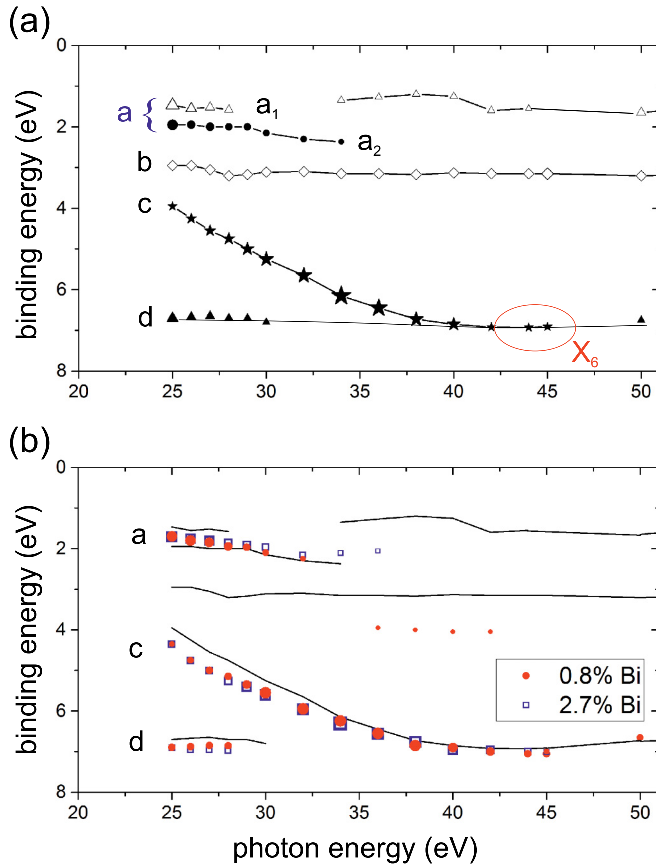

FIG. 12. Dispersion of bands derived from normal emission UPS data in Fig. 11 for (a) pristine GaAs(001)-(2 × 4) and (b) GaAsBi samples. Symbol sizes reflect the intensity of the band signal at respective photon energies. Lines are drawn as a guide to the eye in panel (a), and repeated for comparison in panel (b). All BEs are plotted relative to the appropriate E_{VBM} values in Table I.

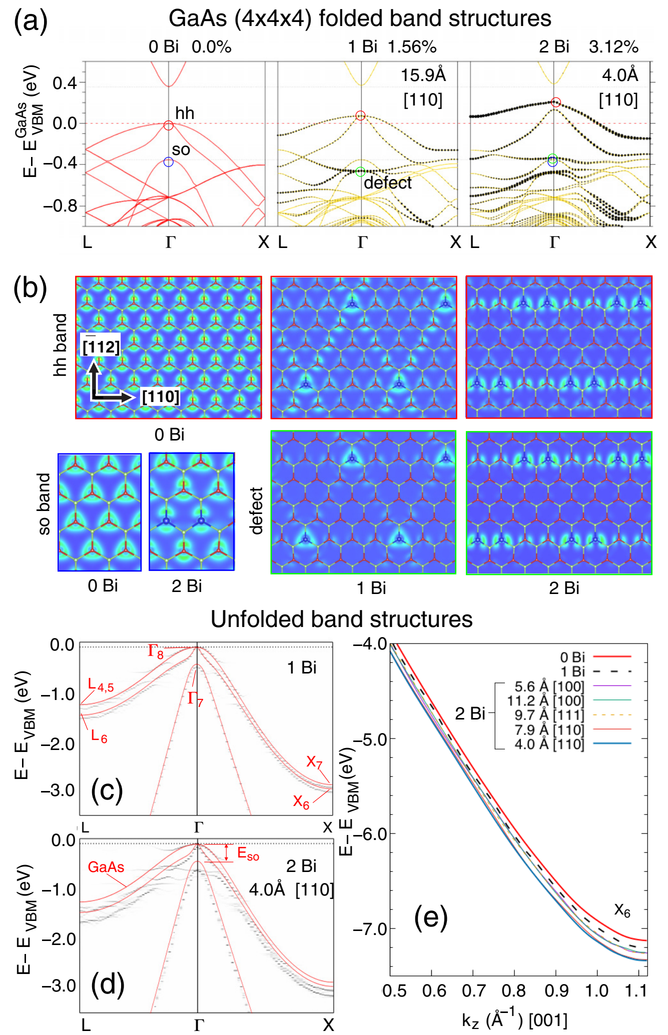

FIG. 13. (a) Folded band structures of GaAs and GaAsBi computed in a $4 \times 4 \times 4$ bulk supercell, for 1 Bi atom ($x = 1.56\%$) and 2 Bi atoms ($x = 3.12\%$) per cell. Bi atoms are aligned along [110] in the latter. Energies are given relative to the valence band maximum (VBM) of pristine GaAs. Black dots indicate contribution from Bi orbitals. (b) Wave functions ($|\psi|^2$) at the Γ point for the same three systems. Heavy hole (*hh*), split-off (*so*), and Bi defect levels are shown as cuts on the $(1\bar{1}1)$ plane through the Bi atoms. Corresponding points are indicated as open circles in (a). Blue, red, and yellow balls indicate Bi, As, and Ga atoms, respectively. (c) Unfolded bands for the 1 Bi and (d) 2 Bi cases, respectively. Bands of pristine GaAs are overlaid in red. Energies are relative to the VBM in each case. (d) Split-off band along Γ–X for increasing Bi composition. Several Bi–Bi orientations and distances are indicated.

picture as broadened disordered bands exhibiting weakened Bloch character. The unfolded *hh* and *lh* bands shift to higher BEs. As shown in Fig. 12(e) (discussed in more detail later), we find a relative shift of the X_6, X_7 points of about 0.1–0.2 eV at 3.12% Bi. (iii) The VBM itself shifts to higher energies with respect to the average bulk potential. This has two effects. First, as the *so* band has a relatively weak Bi contribution [increasing from 1.7% to 3.7% at the Γ point; see Fig. 12(b)], it is barely perturbed. Thus, the split-off energy $\Delta_{\mathrm{SO}}^{\mathrm{GaAs}} = 0.34$ eV concomitantly increases with Bi concentration to 0.43 eV (1 Bi) and 0.56 eV (2 Bi). Similarly, the band gap narrows by 0.07 eV for 1 Bi and 0.21 eV for 2 Bi, with the conduction band remaining fixed in energy. Although we cannot comment on the absolute size of the band gap, the trend is consistent with the experimental photoluminescence gap reduction of 0.16 and 0.27 eV estimated at Bi concentrations of 1.56% and 3.12%, respectively [28], suggesting that the narrowing is a bulk effect. (iv) New defect states (typically 14% localized on Bi) appear below the valence band. For 1 Bi atom, they appear at Γ just below the *so* band at a BE of about 0.6 eV. For higher Bi concentrations, this defect level shifts above the *so* level, and more Bi states appear at deeper levels. These observations are mostly consistent with the unfolded *slab* bands in Fig. 9.

(v) Regarding the real space character of the electronic states, Fig. 13(b) demonstrates the importance of Bi–As and Bi–Bi orbital overlap on the *hh* and defect state character. For the 1 Bi case, the *hh* state retains much of the pure GaAs character in addition to exhibiting intense lobes at the Bi atoms. The last are dominant in the *defect* level. For higher Bi density, the *hh* and defect states become almost indistinguishable in character and show a distinct delocalization along the [110] direction. This points to a hybridization of Bi–As states along

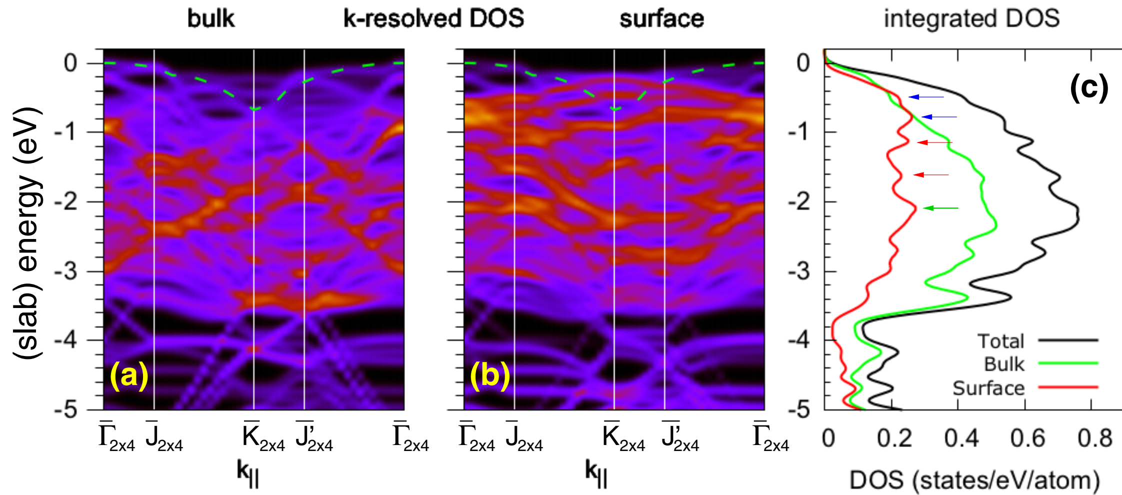

FIG. 14. Density of states of the GaAs(001) slab: k-resolved DOS around the (2×4) surface BZ for (a) bulk and (b) surface atoms only; (c) integrated DOS projected over surface, bulk, and whole slab. The upper limit of the projected bulk band structure is indicated by dashed lines in (a) and (b).

with a strong directional-dependent coupling along the Bi–Bi axis (particularly favoured for this configuration[29]).

The magnitude of the energetic shifts and splittings depends strongly on the Bi–Bi direction and distance [27]. We investigated this for the 3.12% Bi concentration (2 Bi atoms/cell) by considering various Bi–Bi separations and orientations. Note that the 1 Bi case corresponds to a 15.9 Å Bi–Bi pair along [110]. We found that the largest perturbation to the electronic band structure occurs for Bi–Bi pairs aligned along the [110] zigzag chain direction. Figure 13(e) shows the behavior of the Γ–X split-off band at higher photon energies for different Bi–Bi configurations. For the X_6 point around -7 eV, the largest shifts occur for Bi–Bi oriented along [110], although Bi–Bi separations of 4.0 and 7.9 Å yield similar results. For other configurations the effect is less enhanced. The [100]- and [111]-oriented pairs yield the same shift, independent of the Bi–Bi distance. (In these cases the hh and lh bands remain degenerate at the VBM at Γ, and the band gap reduction is about 0.1 eV, i.e., half that of the [110] case). The magnitude of the X_6 shift, 0.1–0.2 eV, is comparable to that observed experimentally in Fig. 12(b). Our bulk supercell calculations therefore succeed in reproducing the basic Bi-induced deformations of the GaAs bands detected in UPS.

The microscopic origin of Bi-induced changes on the band structure has been thoroughly discussed in the literature [27,29–32], and it is useful to put our theoretical findings in the context of previous studies. As we are concerned only with relatively low Bi concentrations (dilute limit), we do not comment on models of band anticrossing or defect band broadening [32] except to recall the observed upwards shift of Bi defect levels at 3.12% Bi in Fig. 13(a). At higher Bi concentrations, the role of configurational disorder also becomes important [27]. The enhanced hh and so state localization along [110] evident in Fig. 13(b) is consistent with the findings of Virkkala *et al.* [29], who reported an agglomeration of the valence band edge charge density along the $\langle 110 \rangle$ directions. Bannow *et al.* [27] suggested this charge density accumulation depends on the hybridization of Bi and As states, which is maximized by a favourable alignment of Bi p orbitals with neighboring As orbitals. This picture is fully consistent with our calculations. The combination of hybridization and charge accumulation thus give rise to shifts in the VBM. As the so and CB states are barely influenced by Bi at this concentration, an increase in Δ_{SO} and a narrowing of the gap E_g follows.

Finally, we consider the surface contribution to the electronic properties. Figure 14 shows the k-resolved DOS and integrated DOS of the $\beta2(2 \times 4)$ reconstructed slab, each projected onto surface and bulk regions as defined in Sec. II B. A number of "true" SSs, i.e., lying within the projected bulk gap, are visible around the $\bar{K}_{2\times4}$ point as previously reported [23,33]. These bands give rise to a peak in the total DOS at -0.5 eV, as indicated by the upper blue arrow in Fig. 14(c). A second peak arising from surface-localized resonance states is observed at -0.8 eV, and is associated with a very flat band along $\bar{\Gamma}$–$\bar{J}_{2\times4}$ in particular and an intense signal around $\bar{\Gamma}$, as seen in Fig. 14(b). It likely corresponds to the flat feature (at -0.8 eV) unfolded to $\bar{J}$ in Fig. 5(h). We tentatively associate these two peaks with the SS shoulder identified in our measured UPS [Fig. 11(a)] and the S_1 and S_2 surface states previously identified in ARPES data by Larsen *et al.* [20]. Further peaks in the integrated surface DOS are observed at -1.2, -1.6, and -2.1 eV. They arise from various resonances dispersing weakly along $\bar{\Gamma}$–$\bar{J}_{2\times4}$ (compare to the unfolded bands in Fig. 9). The latter states are thus well consistent with the a_1 and a_2 UPS features. We are not, however, able to make a clear interpretation of band b, due to the considerable overlap with bulk states within the relevant energy range (2.5–3.5 eV).

VI. SUMMARY

We studied the structural and electronic properties of molecular beam epitaxy grown $GaAs_{1-x}Bi_x$ with (001) surface orientation for varying Bi concentrations. Band structure properties of the well-known $\beta2(2 \times 4)$ reconstruction of pure GaAs(001) were measured by angle-resolved photoemission

as well as photon-energy-dependent ultraviolet photoemission spectroscopy.

By comparing the experimental data to density functional theory calculations of bulk GaAs and the $\beta 2(2 \times 4)$-reconstructed GaAs surface, we have shown that angle-resolved photoemission intensities at 21.2 eV photon energy are governed by projections of bulk heavy and light hole bands in an extended Brillouin zone scheme along the high-symmetry directions X-W-X′, X-U-Γ′, Γ-K-X′, and Γ-L-Γ. Analysis of the k_z dependence is crucial. From the slab calculation we attribute an experimentally observed (and previously unreported) dispersing band at binding energies of about 1 eV with a surface state. k-PEEM and highly resolved ultraviolet photoemission spectroscopy measurements at synchrotron facilities reveal that the integration of Bi into GaAs leads to a broadening of the band structure and a shift in the dispersion of GaAs bulk heavy hole and light hole bands. Bi atoms are found to be integrated as a Bi-rich surface layer and bulk Bi species which lead to a change of the surface order towards a (2×3) symmetry. We achieved Bi bulk concentrations of up to 1.3 at. % while preserving surface order and high crystallinity. Bi-induced energy shifts and broadening effects of the GaAs heavy and light hole bulk bands become evident in photoemission measurements. These findings are reproduced in DFT calculations where low concentrations of Bi are substituted for bulk or subsurface As atoms. Bi-induced electronic band structure effects underlines the potential of $GaAs_{1-x}Bi_x$ compounds for modulations in the optical band gap and thus optoelectronic applications.

ACKNOWLEDGMENTS

This study was supported by the Bilateral Mobility Program between CNR (SAC.AD002.018.017) (Italy) and the Czech Academy of Sciences (CNR-16-02) and by the project Consolidate the Foundation 2015 - *BILLY* - of the University of Rome Tor Vergata. C.H. acknowledges CINECA under the ISCRA scheme and the North-German Supercomputing Alliance (HLRN) for high-performance supercomputing resources and support that have contributed to the research results reported in this paper. Experimental work was supported by the Ministry of Education, Youth and Sports (MEYS), projects LO 1409, LM2015088, and CZ.02.1.01/0.0/0.0/16-013/0001406. The research leading to this result has been supported by the project CALIPSOplus under Grant Agreement No. 730872 from the EU Framework Program for Research and Innovation HORIZON 2020. We particularly thank Mathias Gehlmann for valuable discussions.

Samples were grown and characterized by E.P. and F.A.; Photoemission and k-PEEM measurements were performed by M.V., Y.P., and J.H. with the contribution of E.P., J.K., and F.A; C.H. performed all the theoretical calculations. The paper was written by J.H., C.H., E.P., and F.A., with the help and through contributions from all co-authors. All authors have given approval to the final version of the manuscript. The project was initiated and conceptualized by J.H., E.P., and F.A.

APPENDIX A: XPS EVALUATION PROCEDURES

Table II reports the fitting parameters used in the program KOLXPD [https://www.kolibrik.net/kolxpd]. Voigt peaks on a linear background were used for fitting. A broad peak appears at about 155.5 eV, which corresponds to a loss satellite from As $3p$ CLs. It is displayed as part of background and not discussed later. The estimation of the relative concentrations between Bi $4f$-1, Bi $4f$-2, and Ga $3s$ in Fig. 4(b) is based on respective Voigt peak areas, which are normalized to calculated photoionization cross sections [34]. Respective estimations of relative Ga and As concentrations derived from Ga $3d$ and As $3d$ peak intensities in Figs. 3(a) and 3(b) is about 1:1 within the error margins.

Chemical shifts of the Bi $4f$-2 doublet with respect to the Bi $4f$-1 doublet were found stable at +0.8 eV for all spectra. Lorentzian widths of Bi $4f$ CLs were stable around 0.5 eV; respective Gaussian widths vary from about 0.45 to 0.70 eV for sputtered and sputter-annealed surfaces.

TABLE III. Top: Band structure parameters of bulk GaAs as a function of exchange-correlation functional. LDA calculations use ultrasoft pseudopotentials [12]; PBE, and PBEsol use norm-conserving types [40]. Spin orbit coupling is included throughout. Energies are reported in eV relative to the valence band maximum. Bottom: Lattice constants of GaAs and GaBi. GW and experimental data are compiled from Ref. [37]; the GaBi lattice constant is an extrapolation of $GaAs_{1-x}Bi_x$ alloy data [41].

		LDA	PBE	PBEsol	GW	Expt.
E_g	Γ_{6c}	0.36	0.06	0.42	1.31	1.52, 1.63
E_{VBM}	Γ_6	0.00	0.00	0.00	0.00	0.00
Δ_{so}	Γ_7	−0.35	−0.33	−0.34	−0.35	−0.34
VBW	Γ_8	−12.73	−12.51	−12.84	−12.53	−13.8,−13.1
	$L_{4,5}$	−1.20	−1.08	−1.15	−1.14	−1.4,−1.3
	L_6	−1.41	−1.28	−1.36	−1.36	
	L_6	−6.96	−6.50	−6.77	−6.68	−7.1,−6.7
	L_6	−11.24	−10.89	−11.08	−10.96	−12.0,−11.24
	X_7	−2.85	−2.58	−2.75	−2.76	−2.8,−2.5
	X_6	−2.95	−2.67	−2.83	−2.84	
	X_6	−7.12	−6.71	−6.93	−6.79	−7.1,−6.7
	X_6	−10.48	−10.21	−10.34	−10.29	− 10.7
GaAs	a_0	5.61	5.75	5.66	–	5.65
GaBi	a_0	6.29	6.49	6.37	–	6.234

APPENDIX B: ROLE OF EXCHANGE-CORRELATION FUNCTIONAL

Table III reports selected band structure parameters of bulk GaAs obtained using various DFT exchange-correlation functionals: LDA, Perdew-Burke-Ernzerhof (PBE) [35] generalized gradient approximation (GGA), and PBE modified for solids (PBEsol) [36]. These data are compared to state-of-the-art quasiparticle GW calculations from Ref. [37], and experimental data.

For occupied states lying within 4 eV of the valence band maximum (VBM), the different methods yield values that are fairly consistent and agree well with the GW results. Although PBEsol reproduces the GW data best, our LDA calculations differ at most by 0.1 eV, justifying our choice of LDA for computing the valence bands of GaAs. PBE consistently yields the poorest results. Computed values in this range are generally in good agreement with published experimental data and our measured *k*-PEEM data in Fig. 5. Notably, the split-off energy Δ_{SO} is well reproduced. At energies further from the VBM, discrepancies are larger, with LDA and PBEsol differing from GW data by up to 0.3 eV. Large deviations are found with respect to the experimental valence band width (VBW).

Table III also reports the computed lattice constants a_0 for GaAs and (zinc-blende) GaBi. In both cases, PBE significantly overestimates a_0, while LDA and PBEsol give reasonable values. Exclusion of SOC in the GaBi case leads to errors of 0.04 Å.

For completeness, we also report in Table III the calculated band gaps of bulk GaAs. As expected, the standard DFT functionals greatly underestimate the measured value of 1.52 eV. Within *ab initio* schemes, improved values can be obtained using the GW approach ($E_g = 1.31$ eV [37]), hybrid functionals ($E_g = 1.29$ eV [38]), or meta-GGAs ($E_g = 1.64$ eV [39]). The last of these has been used for studying band gap modifications in GaAsBi [27].

[1] I. P. Marko, C. A. Broderick, S. Jin, P. Ludewig, W. Stolz, K. Volz, J. M. Rorison, E. P. O'Reilly, and S. J. Sweeney, Optical gain in GaAsBi/GaAs quantum well diode lasers, Sci. Rep. **6**, 28863 (2016).

[2] R. D. Richards, F. Bastiman, J. S. Roberts, R. Beanland, D. Walker, and J. P. R. David, MBE grown GaAsBi/GaAs multiple quantum well structures: Structural and optical characterization, J. Cryst. Growth **425**, 237 (2015).

[3] K. Yamashita, M. Yoshimoto, and K. Oe, Temperature-insensitive refractive index of GaAsBi alloy for laser diode in WDM optical communication, Phys. Status Solidi **3**, 693 (2006).

[4] S. Francoeur, M.-J. Seong, A. Mascarenhas, S. Tixier, M. Adamcyk, and T. Tiedje, Band gap of $GaAs_{1-x}Bi_x$, $0 < x <$ 3.6%, Appl. Phys. Lett. **82**, 3874 (2003).

[5] R. N. Kini, L. Bhusal, A. J. Ptak, R. France, and A. Mascarenhas, Electron Hall mobility in GaAsBi, J. Appl. Phys. **106**, 043705 (2009).

[6] D. L. Sales, E. Guerrero, J. F. Rodrigo, P. L. Galindo, A. Yáñez, M. Shafi, A. Khatab, R. H. Mari, M. Henini, S. Novikov, M. F. Chisholm, and S. I. Molina, Distribution of bismuth atoms in epitaxial GaAsBi, Appl. Phys. Lett. **98**, 101902 (2011).

[7] B. Krömker, M. Escher, D. Funnemann, D. Hartung, H. Engelhard, and J. Kirschner, Development of a momentum microscope for time resolved band structure imaging, Rev. Sci. Instrum. **79**, 053702 (2008).

[8] E. A. Kraut, R. W. Grant, J. R. Waldrop, and S. P. Kowalczyk, Precise Determination of the Valence-Band Edge in X-Ray Photoemission Spectra: Application to Measurement of Semiconductor Interface Potentials, Phys. Rev. Lett. **44**, 1620 (1980).

[9] S. P. Svensson, J. Kanski, T. G. Andersson, and P. O. Nilsson, Photoemission studies of the band bending on MBE-grown GaAs(001), J. Vac. Sci. Technol. B: Microelectron. Nanom. Struct. **2**, 235 (1984).

[10] P. Giannozzi, O. Andreussi, T. Brumme, O. Bunau, M. Buongiorno Nardelli, M. Calandra, R. Car, C. Cavazzoni, D. Ceresoli, M. Cococcioni, N. Colonna, I. Carnimeo, A. Dal Corso, S. de Gironcoli, P. Delugas, R. A. DiStasio, A. Ferretti, A. Floris, G. Fratesi, G. Fugallo, R. Gebauer, U. Gerstmann, F. Giustino, T. Gorni, J. Jia, M. Kawamura, H.-Y. Ko, A. Kokalj, E. Küçükbenli, M. Lazzeri, M. Marsili, N. Marzari, F. Mauri, N. L. Nguyen, H.-V. Nguyen, A. Otero-de-la Roza, L. Paulatto, S. Poncé, D. Rocca, R. Sabatini, B. Santra, M. Schlipf, A. P. Seitsonen, A. Smogunov, I. Timrov, T. Thonhauser, P. Umari, N. Vast, X. Wu, and S. Baroni, Advanced capabilities for materials modeling with QUANTUM ESPRESSO, J. Phys.: Condens. Matter **29**, 465901 (2017).

[11] A. Dal Corso and A. M. Conte, Spin-orbit coupling with ultrasoft pseudopotentials: Application to Au and Pt, Phys. Rev. B **71**, 115106 (2005).

[12] A. M. Rappe, K. M. Rabe, E. Kaxiras, and J. D. Joannopoulos, Optimized pseudopotentials, Phys. Rev. B **41**, 1227 (1990).

[13] F. Bastiman, A. G. Cullis, J. P. R. David, and S. J. Sweeney, Bi incorporation in GaAs(100)-2 × 1 and 4 × 3 reconstructions investigated by RHEED and STM, J. Cryst. Growth **341**, 19 (2012).

[14] P. V. C. Medeiros, S. Stafström, and J. Björk, Effects of extrinsic and intrinsic perturbations on the electronic structure of graphene: Retaining an effective primitive cell band structure by band unfolding, Phys. Rev. B **89**, 041407(R) (2014).

[15] P. V. C. Medeiros, S. S. Tsirkin, S. Stafström, and J. Björk, Unfolding spinor wave functions and expectation values of general operators: Introducing the unfolding-density operator, Phys. Rev. B **91**, 041116(R) (2015).

[16] P. Laukkanen, M. P. J. Punkkinen, A. Lahti, J. Puustinen, M. Tuominen, J. Hilska, J. Mäkelä, J. Dahl, M. Yasir, M. Kuzmin, J. R. Osiecki, K. Schulte, M. Guina, and K. Kokko, Local variation in Bi crystal sites of epitaxial GaAsBi studied by photoelectron spectroscopy and first-principles calculations, Appl. Surf. Sci. **396**, 688 (2017).

[17] Y. Q. Cai, A. P. J. Stampfl, J. D. Riley, R. C. G. Leckey, B. Usher, and L. Ley, Two-dimensional electronic structure $E_i(k_i^{\parallel}), k_i^{\perp})$ of GaAs(001) studied by angle-resolved photoemission, Phys. Rev. B **46**, 6891 (1992).

[18] T. C. Chiang, R. Ludeke, and M. Aono, Angle-resolved photoemission studies of GaAs (100) surfaces grown by molecular-beam epitaxy, Phys. Rev. B **27**, 4770 (1983).

[19] J. Olde, G. Mante, H.-P. Barnscheidt, L. Kipp, J.-C. Kuhr, R. Manzke, M. Skibowski, J. Henk, and W. Schattke, Electronic structure of GaAs(001), Phys. Rev. B **41**, 9958 (1990).

[20] P. K. Larsen and J. D. van der Veen, Surface band structure of MBE-grown GaAs(001)-2 $\times$ 4, J. Phys. C Solid State Phys. **15**, L431 (1982).

[21] E. Placidi, C. Hogan, F. Arciprete, M. Fanfoni, F. Patella, R. Del Sole, and A. Balzarotti, Adsorption of molecular oxygen on GaAs(001) studied using high-resolution electron energy-loss spectroscopy, Phys. Rev. B **73**, 205345 (2006).

[22] F. Arciprete, C. Goletti, E. Placidi, C. Hogan, P. Chiaradia, M. Fanfoni, F. Patella, and A. Balzarotti, Surface states at the GaAs(001)-2 $\times$ 4 surface, Phys. Rev. B **69**, 081308 (2004).

[23] W. G. Schmidt and F. Bechstedt, Geometry and electronic structure of GaAs(001)(2 $\times$ 4) reconstructions, Phys. Rev. B **54**, 16742 (1996).

[24] S. Souma, L. Chen, R. Oszwałdowski, T. Sato, F. Matsukura, T. Dietl, H. Ohno, and T. Takahashi, Fermi level position, Coulomb gap and Dresselhaus splitting in (Ga,Mn)As, Sci. Rep. **6**, 27266 (2016).

[25] H. Kumigashira, H.-D. Kim, T. Ito, A. Ashihara, T. Takahashi, T. Suzuki, M. Nishimura, O. Sakai, Y. Kaneta, and H. Harima, High-resolution angle-resolved photoemission study of LaSb, Phys. Rev. B **58**, 7675 (1998).

[26] J. Kanski, L. Ilver, K. Karlsson, I. Ulfat, M. Leandersson, J. Sadowski, and I. Di Marco, Electronic structure of (Ga,Mn)As revisited, New J. Phys. **19**, 023006 (2017).

[27] L. C. Bannow, O. Rubel, S. C. Badescu, P. Rosenow, J. Hader, J. V. Moloney, R. Tonner, and S. W. Koch, Configuration dependence of band-gap narrowing and localization in dilute $GaAs_{1-x}Bi_x$ alloys, Phys. Rev. B **93**, 205202 (2016).

[28] X. Lu, D. A. Beaton, R. B. Lewis, T. Tiedje, and Y. Zhang, Composition dependence of photoluminescence of $GaAs_{1-x}Bi_x$ alloys, Appl. Phys. Lett. **95**, 041903 (2009).

[29] V. Virkkala, V. Havu, F. Tuomisto, and M. J. Puska, Modeling Bi-induced changes in the electronic structure of $GaAs_{1-x}Bi_x$ alloys, Phys. Rev. B **88**, 235201 (2013).

[30] O. Rubel, A. Bokhanchuk, S. J. Ahmed, and E. Assmann, Unfolding the band structure of disordered solids: From bound states to high-mobility Kane fermions, Phys. Rev. B **90**, 115202 (2014).

[31] M. Usman, C. A. Broderick, A. Lindsay, and E. P. O'Reilly, Tight-binding analysis of the electronic structure of dilute bismide alloys of GaP and GaAs, Phys. Rev. B **84**, 245202 (2011).

[32] H.-X. Deng, J. Li, S.-S. Li, H. Peng, J.-B. Xia, L.-W. Wang, and S.-H. Wei, Band crossing in isovalent semiconductor alloys with large size mismatch: First-principles calculations of the electronic structure of Bi and N incorporated GaAs, Phys. Rev. B **82**, 193204 (2010).

[33] C. Hogan, D. Paget, Y. Garreau, M. Sauvage, G. Onida, L. Reining, P. Chiaradia, and V. Corradini, Early stages of cesium adsorption on the As-rich $c(2 \times 8)$ reconstruction of GaAs(001): Adsorption sites and Cs-induced chemical bonds, Phys. Rev. B **68**, 205313 (2003).

[34] J. J. Yeh and I. Lindau, Atomic subshell photoionization cross sections and asymmetry parameters: $1 \leqslant Z \leqslant 103$, At. Data Nucl. Data Tables **32**, 1 (1985).

[35] J. P. Perdew, K. Burke, and M. Ernzerhof, Generalized Gradient Approximation Made Simple, Phys. Rev. Lett. **77**, 3865 (1996).

[36] J. Perdew, A. Ruzsinszky, G. Csonka, O. Vydrov, G. Scuseria, L. Constantin, X. Zhou, and K. Burke, Restoring the Density-Gradient Expansion for Exchange in Solids and Surfaces, Phys. Rev. Lett. **100**, 136406 (2008).

[37] B. D. Malone and M. L. Cohen, Quasiparticle semiconductor band structures including spin-orbit interactions, J. Phys.: Condens. Matter **25**, 105503 (2013).

[38] J. Paier, M. Marsman, K. Hummer, G. Kresse, I. C. Gerber, and J. G. Ángyán, Screened hybrid density functionals applied to solids, J. Chem. Phys. **124**, 154709 (2006).

[39] F. Tran and P. Blaha, Accurate Band Gaps of Semiconductors and Insulators with a Semilocal Exchange-Correlation Potential, Phys. Rev. Lett. **102**, 226401 (2009).

[40] M. J. van Setten, M. Giantomassi, E. Bousquet, M. J. Verstraete, D. R. Hamann, X. Gonze, and G.-M. Rignanese, The PseudoDojo : Training and grading a 85 element optimized norm-conserving pseudopotential table, Comput. Phys. Commun. **226**, 39 (2018).

[41] A. Janotti, S.-H. Wei, and S. B. Zhang, Theoretical study of the effects of isovalent coalloying of Bi and N in GaAs, Phys. Rev. B **65**, 115203 (2002).

Correction: The penultimate sentence of the Acknowledgments contained an error and has been set right.